ACS APPLIED MATERIALS & INTERFACES

Research Article

Cite This: ACS Appl. Mater. Interfaces 2018, 10, 44768−44775

www.acsami.org

Blue-Light-Emitting Photostable Hybrid Films for High-Efficiency Large-Area Light Converter and Photonic Applications

Jung-Soo Kang,[†] Jun-Gill Kang,[‡,§] Youngku Sohn,[*,‡] and Kam Tong Leung[*,†]

[†]WATLab and Department of Chemistry, University of Waterloo, Waterloo, Ontario N2L 3G1, Canada

[‡]Department of Chemistry, Chungnam National University, Daejeon 34134, Republic of Korea

[§]ReSEAT Program, Korea Institute Science and Technology Information, Daejeon 34141, Republic of Korea

Supporting Information

ABSTRACT: A blue fluorophore of Schiff base zinc complex is prepared by a hydrolysis-free solution-based synthetic method. Under ultraviolet (UV) excitation, the complex produces blue emission with a quantum yield (Q) of 42.6% in methylene chloride and 24.0% in standalone powder form. Quantum mechanical calculations show that the blue emission is generated by the change in the chemical state of the ligand associated with the complexation with Zn cations. Thin films of Zn complexes incorporated in polymethylmethacrylate (PMMA) and cellulose acetate butyrate (CAB) polymers are also prepared by dispersing the complexes into the polymer matrices. These hybrid polymer films exhibit several notable features, particularly enhanced luminescence efficiency (with maximum Q of 85.8% for PMMA and 30.0% for CAB) and scalability for fabrication over a large area while retaining the original properties of the host polymers. Light-emitting diodes are also fabricated using the CAB hybrid thin films, and they show a Q of 43.2% with excellent photostability. The complex and its hybrid films demonstrate their great potential for such applications as UV-to-blue conversion devices in photoelectronics, solar-cell concentrators, solid-state lighting and display, and greenhouse agriculture.

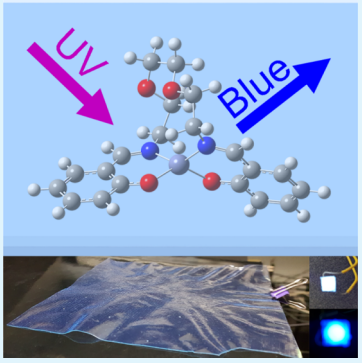

KEYWORDS: *fluorescent polymer films, blue emission, Schiff base, photostable hybrid films*

INTRODUCTION

The design and fabrication of fluorescent organic materials, especially in the form of metal complex−polymer hybrid films, have drawn special attention as potential light converters for application in solid-state lighting and display, photovoltaics, bioimaging, chemo-sensing, and greenhouse agriculture.[1−16] Among them, ultraviolet (UV)-to-blue converting fluorescent polymer films have been particularly attractive as they utilize the UV part of the solar radiation as fluorescent solar concentrators. The global solar radiation that reaches the Earth's surface contains UV, photosynthetically active radiation, and near-infrared radiation. Although the photosynthetically active radiation (400−700 nm) is needed for photosynthesis and plant growth, most plants have their maximal photosynthetic sensitivity in the dark blue (455−500 nm), light blue (485−505 nm), and red (620−760 nm) regions.[17] On the other hand, UV radiation, specifically UV-A (320−400 nm), produces significantly reduced photosynthetic performance.[18] UV-to-blue conversion can therefore provide a vitally important pathway for plant growth.

In recent years, blue-light-emitting polymer films have also been considered as alternatives to inorganic materials for phosphor-converted white-light-emitting diodes (pc-WLEDs) because of their ease of large-scale synthesis and fabrication into devices.[19−24] The first commercially available pc-WLEDs were based on the combination of a blue GaN LED chip with yellow phosphor, such as modified YAG:Ce^{3+}.[25] However, these two-color pc-WLEDs showed a low color rendering index and a highly correlated color temperature. To overcome the drawbacks of the two-color pc-WLEDs, some attempts have been made by adding appropriate red phosphors to the yellow phosphor or by combining green and red phosphors with blue LED chips.[26−28] These modified two-color pc-WLEDs, however, exhibited intensity leakage of the blue light, because the supplemented phosphors also converted the remainder of the blue light wavelength into the red and green spectral components. Recent developments of LED chip technology have led to greater availability of the 365 nm near-UV chips with higher power and lower cost than the shorter-wavelength UV LEDs.[29] The combination of near-UV LED with red·green·blue (RGB) phosphors also offers notable advantages, such as high efficiency, high color rendering index, and high chromatic stabilities, when compared to the aforementioned LEDs.[30−32] To date, the commercial availability of blue phosphors to satisfy the spectral requirements of the 365 nm excitation has remained very limited. The preparation of blue fluorescent materials via a simple synthetic method that gives good yield and uses only commercially

Received: October 10, 2018
Accepted: November 28, 2018
Published: November 28, 2018

DOI: 10.1021/acsami.8b17256
ACS Appl. Mater. Interfaces 2018, 10, 44768−44775

available starting materials will therefore be of great interest and is expected to have significant impact on the commercial application of pc-WLEDs, UV-to-blue conversion, and other solid-state lighting technology and devices.[33−38]

Metal−organic ligand complexes have been extensively studied for luminescent applications because of their superior stability and relatively easy synthesis. Among them, lanthanide (Ln) ions, specifically Tb(III) and Eu(III), have been considered key components for designing green and red luminescent materials because they possess several unique luminescence properties, including hypersensitivity to their coordination environments, good color representation with narrow bandwidth, and millisecond luminescence lifetimes. Furthermore, the drawback arising from a very small f → f absorption coefficient can be overcome by introducing organic ligands as sensitizers.[1,39−43] However, no Ln(III) ions appropriate for emitting a pure blue light have been reported. Only a handful of Ln(III) complexes based on a few ligands, such as 1,8-naphthalimide derivatives, 1,3,5-benzenetricarboxylic acid, poly(styrene-coglycidyl methacrylate), 1,10-phenanthroline, and *N*,*N*′-bis(salicylidene)-3,6-dioxa-1,8-diaminooctane (LH_2), have been realized as UV-to-red or UV-to-green conversion components.[1,42−44] In these complexes, the ligands play a key role in generating the light emissions. For example, the sensitized emission of Eu(III) complexes based on LH_2 is mainly generated by an energy transfer from the L ligand, even though LH_2 itself is not luminescent.[39]

In this study, a Schiff base, LH_2, is used to form a complex with zinc. The photophysical properties, thermal stability, and photostabilities of the resulting zinc(*N*,*N*′-bis(salicylidene)-3,6-dioxa-1,8-diaminooctane) (ZnL) fluorophore and of the polymer films hybridized with ZnL are investigated. For the hybrid films, polymethylmethacrylate (PMMA) and cellulose acetate butyrate (CAB) are selected as the host polymers. PMMA is one of the most common matrices used for incorporating metal−organic ligand complexes to enhance the photostabilities of selected metal complexes.[45,46] Like PMMA, CAB also has very attractive properties, such as biocompatibility, high transparency, and a high film-forming capacity. In addition, CAB is not only thermally stable to 300 °C but also photochemically stable for (UV) wavelength longer than 280 nm.[47,48] In addition, quantum mechanical calculations using density function theory (DFT) and Zerner's intermediate neglect of differential overlap (ZINDO) are performed to obtain the equilibrium geometries. The calculated electronic structures for LH_2 and the ZnL complex are used to investigate the origin of the observed blue emission and their photophysical properties. Finally, we fabricate a pc-LED by combining the hybrid film with an InGaN LED chip, and we demonstrate the performance of the resulting blue LED and its viability for use as a near-UV-light conversion device.

RESULTS AND DISCUSSION

It is well known that the hydrolysis reaction is one of the main challenges in preparing Schiff-base metal complexes. This is because hydrolysis causes chemical decomposition during the synthesis and purification process of metal complexes.[49] We perform a series of systematic experiments involving multiple organic solvents with various metal nitrates (Supporting Information). Among them, the ZnL complex is synthesized by using zinc nitrate, and the synthesized complex is found to be chemically stable during the synthesis and purification processes. The hydrolysis-free synthesis also has a high production yield (>95%), and the resulting complex exhibits very bright blue luminescence. Its chemical nature is confirmed by elemental analysis, ^{1}H nuclear magnetic resonance, and Fourier transform infrared (FT-IR) spectra (Supporting Information). Thermal gravimetric (TG) and differential thermal analysis (DTA) profiles of the ZnL complex, recorded up to 800 °C, are shown in Figure S1. No distinct weight loss is observed until 280 °C for the ZnL complex, indicating that the ZnL complex is thermally stable at least up to 250 °C.

Hybrid films are also prepared by incorporating different amounts of ZnL into PMMA and CAB polymer matrices. The prepared hybrid films, denoted here as PMMA-*x* (*x* = 0−5 wt % of ZnL) and CAB-*x* (*x* = 0−4 wt % of ZnL), are characterized by FT-IR spectroscopy. The FT-IR spectra of the CAB-0 and CAB-4 films are compared in Figure 1a. Except for

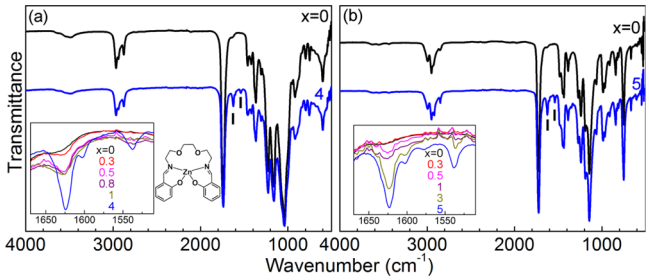

Figure 1. FT-IR spectra of (a) CAB-0 and CAB-4 films and (b) PMMA-0 and PMMA-5 films illustrating the effect of ZnL content on the L characteristic C═N and aromatic C═C stretching bands at 1623 and 1536 cm^{-1}, respectively (identified by short markers and shown on an extended scale in insets). The molecular structure of ZnL is shown in (a) for clarity.

two weak bands at 1624 and 1536 cm^{-1} (Figure 1a inset, discussed below), there is no significant spectral difference between CAB-0 and CAB-4. The weak broad band at 3490 cm^{-1} corresponds to the stretching mode of the OH group attached to the glucose unit. The weak multiplet feature located at 2960−2870 cm^{-1} along with the weak band at 1369 cm^{-1} can be attributed to the CH stretching vibration. Characteristic C−O−C vibrations of the glucose frame and of the β-glycosidic linkage between the glucose units correspond to the strong band at 1040 cm^{-1} and the intermediate feature at 593 cm^{-1}, respectively. The substituted acetate and butyrate groups give rise to the strong feature at 1742 cm^{-1}, assigned as the C═O stretching mode of the ester. The spectra in Figure 1a inset show the effect of ZnL content on the intensities of two additional bands at 1624 and 1536 cm^{-1}, which correspond to, respectively, the C═N and aromatic C═C stretching vibrations of the L ligand in the ZnL complex. With increasing ZnL content, the intensities of these two bands are found to increase. The weak spectral intensity even for the 4.0 wt % ZnL content suggests that the CAB polymer matrix has accommodated the ZnL complex homogeneously and that the ZnL complexes are distributed uniformly without aggregation. For the PMMA-*x* films, similar changes in the ZnL spectral features at 1624 and 1536 cm^{-1} with increasing ZnL content are also observed in the corresponding FT-IR spectra shown in Figure 1b.

We also investigate the photophysical properties of LH_2 and the ZnL complex in conjunction with their molecular structures. Figure 2a shows the UV−vis absorption spectra of LH_2 and ZnL, each dissolved in methylene chloride (MC),

DOI: 10.1021/acsami.8b17256
ACS Appl. Mater. Interfaces 2018, 10, 44768−44775

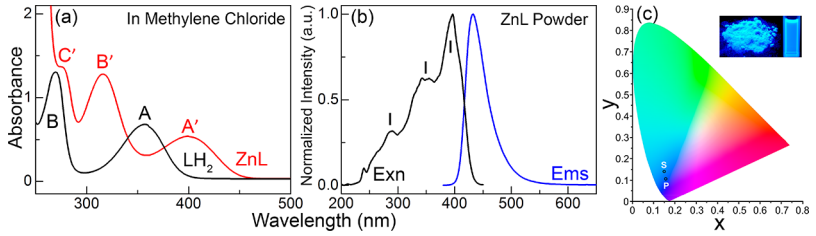

Figure 2. (a) Absorption spectra of LH_2 and ZnL dissolved in MC. (b) Luminescence (Ems, λ_{exn} = 365 nm) and excitation (Exn, λ_{ems} = 480 nm) spectra of ZnL in powder form. (c) CIE chromaticity diagram depicting the color coordinates of ZnL powder (P) and ZnL dissolved in MC (S), with the inset showing a photograph of the powder (left) and dissolved forms (right) of ZnL under UV excitation.

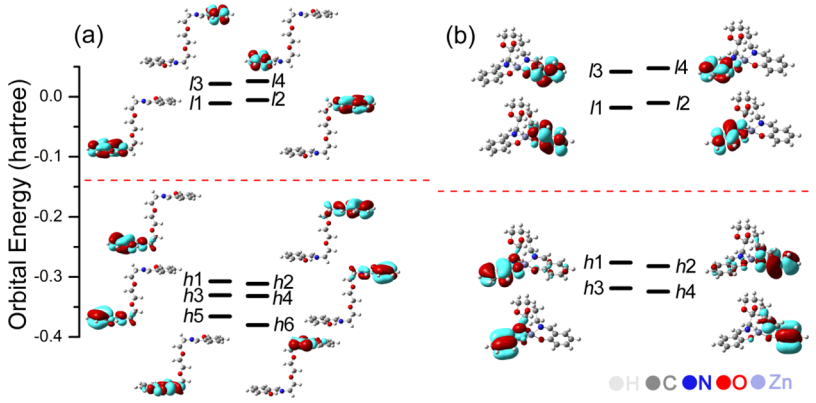

Figure 3. Molecular orbital energy-level diagrams of (a) LH_2 and (b) ZnL with corresponding electron density isocontours.

which evidently appear quite different from each other. Two characteristic bands at 355 and 270 nm (hereafter referred to as A and B bands, respectively) for LH_2 and three bands at 405, 315, and 275 nm bands (hereafter referred to as A′, B′, and C′ bands, respectively) for ZnL are observed. The luminescence spectra of LH_2 and the ZnL complex in powder form are measured upon the A-band excitation (365 nm). Although the LH_2 powder does not exhibit any luminescence, the ZnL powder produces very strong blue emission with a maximum at 447 nm, as shown in Figure 2b. Also shown in Figure 2b is the photoluminescence excitation spectrum of the 480 nm emission. The blue luminescence of ZnL is produced over the entire UV range, with three peaks observed at 390, 340, and 290 nm (identified by markers) corresponding to the A′, B′, and C′ absorption bands, respectively (in Figure 2a). Figure 2c shows the colors of the PL emission from ZnL in powder and in MC phases on the Commission Internationale de l'Éclairage (CIE) 1931 color space. Evidently, ZnL emits blue light in powder form and the color becomes sky blue in the solution phase.

To investigate the mechanism of blue light emission produced by the ZnL complex, quantum mechanical calculations are performed to characterize the observed absorption and emission properties by using Gaussian 09.[50] The equilibrium structures of the LH_2 and ZnL molecules are optimized at the level of DFT/B3LYP/6-31G. In the optimized geometry of LH_2 [$(2\text{-}HOC_6H_4CH{=}NCH_2CH_2OCH_2)_2$] shown in Figure S2, the two salicylidene-amino groups are each positioned perpendicular to the dioxa chain connecting them. For the ZnL complex [$Zn(2\text{-}OC_6H_4CH{=}NCH_2CH_2OCH_2)_2$], the Zn atom is quadruple coordinated via bonding to N and O atoms in each of the two dehydrogenated salicylideneamino groups. Because the center Zn atom is connected to two terminal phenolates, the planar geometry of the complex is twisted.

The electronic structures and transitions are also calculated semiempirically for the first 60 singlet states at the ZINDO level. Details of the calculated highest occupied molecular orbitals (HOMO) and lowest unoccupied molecular orbitals (LUMO) of LH_2 and ZnL are given in Tables S1 and S2, respectively. For LH_2 (Figures 3a and S2a) and ZnL (Figures 3b and S2b), the combinations of the p_x and p_y orbitals of O and N atoms in the two salicylideneamino groups and the π-bonding orbitals from the benzene ring (with two nodal planes) result in the HOMO and three next HOMOs, hereafter referred to as h1−h4. As these orbital components have different parities, this leads to the formation of antibonding character between the benzene ring and the N and O atoms. The contributions of the π-orbitals of the two benzene rings give rise to two sets of nearly doubly degenerate HOMOs for each LH_2 and ZnL. It should be noted that for LH_2 the major contributions to the h5 and h6 orbitals come from lone-pair electron contributions from the N atoms in the form of s and p_z orbitals, and not from the π-orbitals of the benzene rings. For LH_2, the nearly degenerate LUMO l1 and the next LUMO l2, and the nearly degenerate l3 and l4, primarily correspond to the antiphase combinations of different π^* orbitals of the benzene ring with the p_x and p_y orbitals of the nearest N atom in the two salicylideneamino groups. For the ZnL complex, the characters of the two nearly degenerate LUMO pairs, l1 and l2 and l3 and l4, are found to be very similar to the corresponding LUMO pairs of LH_2. Indeed, the presence of the Zn atom in ZnL does not appear to significantly affect the combinations of atomic orbitals in these frontier HOMOs and LUMOs.

The simulated absorption spectra of isolated LH_2 and ZnL molecules are shown in Figure S3. Assuming an arbitrary shift

DOI: 10.1021/acsami.8b17256
ACS Appl. Mater. Interfaces 2018, 10, 44768−44775

of ~50 nm between the gas phase (isolated molecule case) and the condensed phase, the simulated spectra are in good accord with the experimentally observed absorption bands. Excited states and their corresponding oscillator strengths (f-numbers for isolated molecule case), along with the nature of their predominant configurations, for the observed absorption bands of LH_2 and the ZnL complex dissolved in MC (Figure 2a) are listed in Tables S3 and S4, respectively. For LH_2, several excited states are evidently involved in the A absorption band (Table S3). Among them, the first excited state, 1A, and the fourth excited state, 4A, correspond to the electron transitions h5 → l1 and h6 → l2, respectively. These excited states are associated with the rearrangements of contributions from the N lone-pair electrons in combination with the ring electrons. The oscillator strengths of the transitions from the ground state to the 1A and 4A states are too small to contribute significantly to the intensity of the A band. On the other hand, the respective f-numbers (Table S3) for the 2A, 3A, 5A, and 6A excited states are sufficiently large to contribute to the intensities in the A band. Several excited states are involved in the B band. According to their respective f-numbers, the 7A and 8A excited states provide the largest contributions to the B band. For the ZnL complex (Table S4), the 1A and 2A excited states are responsible for the A′ absorption band and they correspond to the h2 → l1 and the h1 → l2 electron transitions, respectively. For the B′ band, the 8A excited state has the largest f-number, whereas the contributions of the 3A and 4A excited states to the B′ band are considerably less. For the C′ band, the transition from the ground state to the 16A excited state provides the largest contribution, whereas the 15A and 22A states also give sizable contributions.

These calculations reveal that the characteristic features of the observed photophysical properties of LH_2 and the ZnL complex are strongly related to the influence of Zn (i.e., its absence or presence) on the nature of the first excited state, 1A. For LH_2, the 1A state is dominated by a nearly forbidden electronic transition from primarily a N orbital (h5) to the π^* anti-bonding orbital of the benzene ring (l1). In the emission process, the transition to an excited state is often followed by cascade non-radiative relaxation to low-lying excited states. The absence of any emission from LH_2 indicates that the potential wall of the 1A excited state acts as a trap, resulting in non-radiative transition from the 1A excited state predominantly back to the ground state. In contrast, for the ZnL complex, the lone-pair electrons of each N atom are involved in the formation of coordination bonding with Zn. The first two excited states, 1A and 2A, corresponding to the $\pi \rightarrow \pi^*$ transitions of the benzene rings, participate in the formation of the A absorption band (Table S4). The f-numbers of these two states are sufficiently large for radiative transitions from these states to the ground states to give rise to strong fluorescence.

The PL spectra of the ZnL complex in powder, solution, and hybrid polymer film phases are measured and are compared in Figure 4a, and their corresponding absolute quantum yields (Q) and the emission lifetimes are given in Table 1. In addition to the apparent red shifts of the PL maxima of the solution and hybrid films from that of pristine powder, broadening of the luminescence bands is also observed. The corresponding CIE x,y coordinates (Figure 4b and Table 1) from the solution and hybrid films also trend toward the red, when compared to that of the powder phase. For the PMMA films, the CIE x coordinate with 0.3 wt % ZnL is 0.1707. By increasing ZnL content to 5.0 wt %, the x-coordinate repositions to a lower

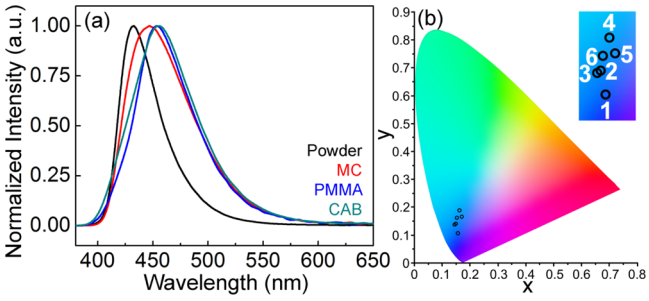

Figure 4. (a) PL spectra of ZnL powder, ZnL dissolved in MC, PMMA-0.5, and CAB-0.8 hybrid films. The peak position and the full width at half maximum are, respectively, 432.2 and 42.2 nm for the powder, 446.8 and 69.6 nm for the solution, 454.0 and 62.7 nm for PMMA-0.5, and 456.0 and 67.8 nm for the CAB-0.8 film. (b) CIE chromaticity diagram for the emission colors of ZnL and its hybrid films. The inset is an expanded view of the CIE diagram for (1) ZnL powder, (2) ZnL dissolved in MC, (3) CAB-0.3, (4) CAB-4, (5) PMMA-0.3, and (6) PMMA-5.

Table 1. Photophysical Properties of ZnL Powder, ZnL in MC Solution, and Hybrid PMMA and CAB Films

				rate constants (1/s)	
sample	CIE (x, y)	Q (%)	τ (ns) (R^2)	$k_r/10^7$	$k_{nr}/10^7$
		ZnL			
powder	(0.1563, 0.1079)	24.0	3.23 (0.999)	7.43	23.5
$\times 10^{-4}$ M	(0.1496, 0.1411)	42.6	8.00 (0.999)	5.30	7.20
		PMMA-x			
0.3	(0.1707, 0.1657)	71.4	4.94 (0.999)	14.4	5.87
0.5	(0.1676, 0.1637)	78.4	4.97 (0.999)	15.8	4.35
1.0	(0.1599, 0.1673)	85.7	5.44 (0.999)	15.7	2.63
3.0	(0.1577, 0.1680)	82.2	5.39 (0.999)	15.3	3.30
5.0	(0.1530, 0.1623)	85.8	4.71 (0.999)	18.2	3.01
		CAB-x			
0.3	(0.1445, 0.1380)	29.6	5.89 (0.999)	5.02	12.0
0.5	(0.1457, 0.1562)	29.3	5.84 (0.999)	5.02	12.1
0.8	(0.1471, 0.1517)	30.0	5.81 (0.999)	5.16	12.1
1.0	(0.1584, 0.1595)	21.7	5.60 (0.999)	3.75	14.1
4.0	(0.1619, 0.1881)	14.7	4.83 (0.999)	3.04	17.7
pc-LED	(0.1700, 0.1929)	43.2			

value of 0.1530, whereas the y-coordinate remains nearly unchanged. This results in the change of the PL color of the PMMA hybrid film from purplish blue to greenish blue. For the CAB hybrid films, the CIE x,y coordinates are distributed over a wider range from (0.1445, 0.1380) for 0.3 wt % ZnL and to (0.1619, 0.1881) for 4 wt %, corresponding to the emission color change from deep blue to sky blue.

The observed quantum yields are 24% for the ZnL powder and 43% for the ZnL 10^{-4} M MC solution phase. The lower quantum yield of the powder is likely because of the emitted blue light from the inner particles not fully scattered to the outside space. These results show that the ZnL powder has a higher quantum yield than that of any blue fluorophore and is therefore superior for application in solid-state UV-light conversion devices, because most of the organic fluorophores (in powder phase) produce very weak fluorescence. There are also significant differences in the quantum yields between the PMMA and CAB hybrid films. For the PMMA hybrid films, the Q value follows an increasing trend from 71 to 86% with ZnL content increasing from 0.3 to 5.0 wt %. These values are

DOI: 10.1021/acsami.8b17256
ACS Appl. Mater. Interfaces 2018, 10, 44768−44775

remarkably high when compared with those of other phases, including the powder, the solution, and the CAB hybrid films. For the ZnL 0.3 wt % hybrid films, the luminescence efficiency of PMMA (71.4%) is more than twice that of CAB (29.6%). By increasing the ZnL content to 0.8 wt % in the CAB hybrid films, Q remains at ∼30%. When the ZnL content reaches 1.0%, Q appears to decrease discernibly to 21.7%, and further to 15% for the CAB-4.0 film. These results suggest that the critical concentration of ZnL for CAB-based hybrid film is 0.8 wt %. In the case of embedding fluorophores into host materials, the receivable area and/or the number of substitutable ions determine the concentration of the dopants.[51,52] The well-accommodated ZnL molecules in the host transfer the energy between ZnL molecules, which enhances the PL intensity. Once the concentration exceeds the critical concentration, the ZnL molecules that are not received do not participate in the energy transfer process, resulting in reduction in the PL intensity and Q. On the other hand, PMMA has a relatively simpler polymer chain and skeleton structure than CAB and can hold more ZnL molecules; therefore, the optimal ZnL content that produces the maximum quantum yield is below 1.0 wt % for the host CAB and above 1.0 wt % for PMMA.

The observed time profile of the luminescence of each sample is well fitted with one exponential decay component, and the decay lifetime (τ) so obtained is summarized in Table 1. The powder phase exhibits the shortest τ, whereas the solution phase gives the longest. For the hybrid films, the concentration dependence of τ follows a similar trend as Q. It suggests that the observed photophysical properties of ZnL in the solution and the hybrid films might be strongly associated with the interaction between the complex and the host medium. The quantum yield can be expressed in terms of radiative (k_r) and non-radiative (k_{nr}) rate constants as[53]

$$Q = \frac{k_r}{k_r + k_{nr}}$$

The rate constants k_r and k_{nr} are calculated using $\tau = 1/(k_r + k_{nr})$, given the ratio k_{nr}/k_r is 3.16 for the powder phase, 1.4 for the solution phase, and 2.34 for the hybrid films.[51] The values for the rate constants are listed in Table 1. The k_r values of the CAB-x (x = 0.3−0.8) films with maximum Q are in the same range as that of the solution phase, whereas there is a large difference in k_{nr} between the hybrid films and the solution phase. The interaction of the ZnL molecule with the CAB unit, involving the OH group and O atoms, is expected to be stronger via the formation of hydrogen bonding, when compared with the case of the MC solution medium. For the CAB polymer film medium, the non-radiative relaxation routes become more active, which results in the reduction of the quantum yield. On the other hand, the k_{nr} values for all of the PMMA-x (x = 0.3−5.0) polymer films (Table 1) are significantly smaller than those of the CAB-x films, which is consistent with the high quantum yields observed for these films.

An important determining factor for the fabrication of the hybrid polymer materials for use in light conversion devices is their photostability against UV light. For the UV aging test, the ZnL powder and hybrid films are placed under UV light illumination from a 10 W UV lamp (365 nm). Figure 5a shows the variation of the peak intensity (I) (with λ_{ems} = 435 nm for the powder and 450 nm for the films) with respect to the initial

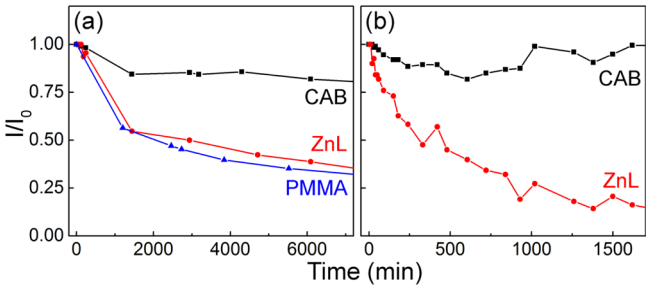

Figure 5. Relative intensity (I/I_0) of the blue emission vs irradiation time for ZnL powder, PMMA-1.0, and CAB-1.0 under irradiation of (a) 10 and (b) 100 W 365 nm UV lamps, with λ_{ems} = 435 nm for the powder phase and 450 nm for the hybrid films.

intensity (I_0) over the irradiation time. The relative intensities of the powder and the PMMA-1.0 hybrid film are found to decrease rapidly to ∼50% upon 20 h irradiation, after which they follow a more gradual decreasing trend to 100 h irradiation. Remarkably, the photostability of ZnL is strongly enhanced in the CAB-1.0 film. For the CAB-1.0 hybrid film, the relative intensity decreases by less than 20% for the first 20 h irradiation, and the intensities remain essentially unchanged to 100 h. To further examine the UV stability of the CAB hybrid film, we employ a 100 W lamp as the UV irradiation source (365 nm). As shown in Figure 5b, similar trends are observed for the 100 W UV irradiation experiments. Although the relative intensity of the ZnL powder decreases steadily to ∼10% after just 25 h of 100 W UV irradiation, that for the CAB hybrid film remains high at 90%. The CAB matrix therefore provides the ZnL molecules good UV protection even under intense UV irradiation.

As the ZnL fluorophore, and the PMMA and CAB matrices have good solubility in many common organic solvents, they are readily compatible for solution processing. Although only a small amount of the ZnL complex is incorporated into the skeletons of PMMA and CAB, the resulting hybrid films not only retain the original polymer properties, such as transparency, flexibility, and adhesiveness, but also exhibit high UV-to-blue conversion efficiencies. These characteristic features are crucial for manufacturing blue-light-emitting films via simple coating, printing, and patterning protocols. Figure 6a shows that the ZnL-CAB hybrid films can emit blue light upon indirect exposure to sunlight (at an average radiation power of 27 μW/cm^2), and the blue emission is easily observable by bare eyes. Under illumination by a 3 W 365 nm UV lamp (with a radiation power of 273 μW/cm^2, i.e., approximately 10 times that of the indirect sunlight), the blue light emission intensifies significantly (Figure 6b). Figure 6c demonstrates the feasibility of large-scale fabrication of a standalone CAB-0.8 film with an approximate area of 300 × 210 mm^2 exposed to the same indirect sunlight as in Figure 6a. This large-scale film is casted on a glass substrate by a simple bar-coating method, and it can be lifted off effortlessly from the substrate. The easily discernible blue light emitted from the entire area of the hybrid film appears uniform. Furthermore, the CAB-0.8 film was exposed to severe condition, by soaking in water at 85 °C for 24 h, in order to assess the stability of the fluorophore and the luminescent polymer film. The photoluminescence intensities before and after the exposure are compared in Figure S4. The minor intensity reduction (less than 9%) after the exposure demonstrates the excellent stability of the fluorophore and its polymer hybrid film. Consequentially, the

DOI: 10.1021/acsami.8b17256
ACS Appl. Mater. Interfaces 2018, 10, 44768−44775

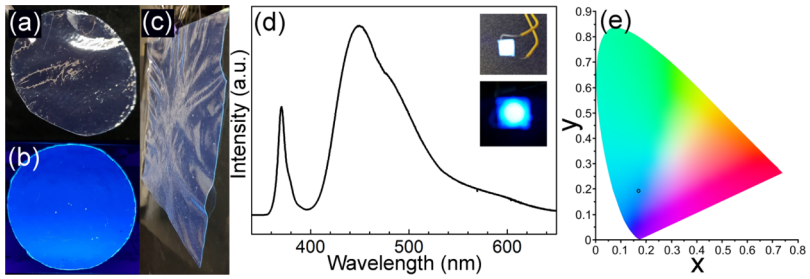

Figure 6. Photographs of CAB-0.8 under irradiation of (a) indirect sunlight (27 μW/cm^2) and (b) 365 nm UV lamp (273 μW/cm^2). (c) Photograph of a large-area CAB-0.8 film (300 × 210 mm^2) excited by indirect sun exposure (27 μW/cm^2). (d) Emission spectrum and photographic images (inset) and (e) CIE chromaticity diagram of the emission color of a pc-LED based on the CAB-0.8 film.

ZnL hybrid film based on CAB is proven readily applicable not just in compact sized applications (such as pc-LEDs, discussed below) but also in such large-area applications as coating for greenhouse glasses to reduce near-UV damages and to enhance the photosynthesis rates for indoor agriculture.

Because the CAB hybrid films demonstrate a remarkable photostability against long UV light exposure, they can be employed as UV-to-blue light convertors to construct blue LEDs. In this study, we apply the CAB-0.8 solution on a quartz plate (6.4 × 6.4 mm^2), and then integrate the coated quartz plate with a 365 nm NUV chip (CUN6AF1B, Seoul Viosys Com.). Figure 6d shows the PL spectrum of the fabricated pc-LED device, which consists of two strong bands. The sharp band at 365 nm and the stronger broad band at 450 nm are attributed to emissions from the pumping InGaN diode and from the ZnL−CAB hybrid film, respectively. From the measured PL spectrum, we estimate the quantum yield of the pc-LED to be 43.2% (Table 1), which is remarkable because it is as high as that obtained from the MC solution phase. The CIE chromaticity diagram for this pc-LED clearly shows that the emission color corresponds to sky blue (Figure 6e).

CONCLUSIONS

For a blue-light-emitting fluorophore, a chemically stable Zn complex with a Schiff base [*N*,*N*′-bis(salicylidene)-3,6-dioxa-1,8-diaminooctane] has been prepared via a facile hydrolysis-free solution-phase reaction. UV excitation of the ZnL complex produces strong blue luminescence in an organic solution (MC) and in the powder phase. In order to realize practical applications for large-area UV-to-blue converters and blue LEDs, we incorporate a small amount of the ZnL fluorophore into PMMA and CAB polymer matrices and characterize their photophysical properties. Although the ZnL PMMA polymer films exhibit high quantum yields (more than three times that of the powder phase), they suffer from poor photostability upon UV illumination. On the other hand, the ZnL-CAB hybrid polymer films retain the luminescence efficiency as much as that of the powder phase but with minimal degradation upon prolonged UV exposure. This remarkable photostability against UV breaching could be caused by the interaction between the ZnL molecule and the OH groups in the CAB skeleton. This is a significant result because the resulting CAB hybrid film can be used as a vital component in UV-to-blue conversion devices (as demonstrated in the present work) and other applications. Manufacturing using such a hybrid film not only is easily scalable and over a large area but also is flexible to a wide range of applications, such as blue LEDs, because the color (emission wavelength) of the emitted blue can be fine-tuned by manipulating the ZnL content.

ASSOCIATED CONTENT

Supporting Information

The Supporting Information is available free of charge on the ACS Publications website at DOI: 10.1021/acsami.8b17256.

Details of experimental procedures and the results of TG/DTA and quantum mechanical calculations (PDF)

AUTHOR INFORMATION

Corresponding Authors

*E-mail: youngkusohn@cnu.ac.kr (Y.S.).
*E-mail: tong@uwaterloo.ca (K.T.L.).

ORCID

Youngku Sohn: 0000-0001-5052-8960
Kam Tong Leung: 0000-0002-1879-2806

Notes

The authors declare no competing financial interest.

ACKNOWLEDGMENTS

J.-S.K. and K.T.L. acknowledge the Natural Sciences and Engineering Research Council of Canada. J.-G.K. acknowledges the ReSEAT program funded by the Ministry of Science, ICT and Future Planning through the National Research Foundation of Korea, and the Korea Lottery Commission grants. Y.S. acknowledges National Research Foundation of Korea (NRF) grant funded by the Korea government (MEST) (2016R1D1A3B04930123).

REFERENCES

(1) Wei, H.; Zhao, Z.; Wei, C.; Yu, G.; Liu, Z.; Zhang, B.; Bian, J.; Bian, Z.; Huang, C. Antiphotobleaching: A Type of Structurally Rigid Chromophore Ready for Constructing Highly Luminescent and Highly Photostable Europium Complexes. *Adv. Funct. Mater.* **2016**, *26*, 2085−2096.

(2) Zhang, T.; Sun, J.; Liao, X.; Hou, M.; Chen, W.; Li, J.; Wang, H.; Li, L. Poly(9,9-dioctylfluorene) Based Hyperbranched Copolymers With Three Balanced Emission Colors for Solution-processable Hybrid White Polymer Light-emitting Devices. *Dyes Pigm.* **2017**, *139*, 611−618.

(3) Yang, W.; Wang, X.; Wang, S.; Hao, W. White-light-emitting Hybrid Film from Fluorescent Hyperbranched Poly(amido amine). *J. Appl. Polym. Sci.* **2017**, *135*, 46015.

(4) Gotta, J.; Shalom, T. B.; Aslanoglou, S.; Cifuentes-Rius, A.; Voelcker, N. H.; Elnathan, R.; Shoseyov, O.; Richter, S. Stable White Light-Emitting Biocomposite Films. *Adv. Funct. Mater.* **2018**, *28*, 1706967.

DOI: 10.1021/acsami.8b17256
ACS Appl. Mater. Interfaces 2018, 10, 44768−44775

(5) Li, W.; Hendriks, K. H.; Furlan, A.; Roelofs, W. S. C.; Meskers, S. C. J.; Wienk, M. M.; Janssen, R. A. J. Effect of the Fibrillar Microstructure on the Efficiency of High Molecular Weight Diketopyrrolopyrrole-Based Polymer Solar Cells. *Adv. Mater.* **2013**, *26*, 1565−1570.
(6) Cheng, P.; Zhan, X. Stability of Organic Solar Cells: Challenges and Strategies. *Chem. Soc. Rev.* **2016**, *45*, 2544−2582.
(7) Smirnov, J. R. C.; Zhang, Q.; Wannemacher, R.; Wu, L.; Casado, S.; Xia, R.; Rodriguez, I.; Cabanillas-González, J. Flexible All-polymer Waveguide for Low Threshold Amplified Spontaneous Emission. *Sci. Rep.* **2016**, *6*, 34565.
(8) Tian, W.; Zhang, J.; Yu, J.; Wu, J.; Nawaz, H.; Zhang, J.; He, J.; Wang, F. Cellulose-Based Solid Fluorescent Materials. *Adv. Opt. Mater.* **2016**, *4*, 2044−2050.
(9) Kim, D.; Kwon, J. E.; Park, S. Y. Is Color-Specific Photoswitching in Dual-Color Fluorescence Systems Possible? Manipulating Intermolecular Energy Transfer among Two Different Fluorophores and One Photoswitch. *Adv. Opt. Mater.* **2016**, *4*, 790−797.
(10) Blasi, D.; Nikolaidou, D. M.; Terenziani, F.; Ratera, I.; Veciana, J. Excimers from Stable and Persistent Supramolecular Radical-pairs in Red/NIR-emitting Organic Nanoparticles and Polymeric Films. *Phys. Chem. Chem. Phys.* **2017**, *19*, 9313−9319.
(11) Ding, W.; Zhang, G.; Zhang, H.; Xu, J.; Wen, Y.; Zhang, J. One Step Electrosynthesis of Conjugated Polymers Thin Film for Fe^{3+} Detection and Its Potential Application. *Sens. Actuators, B* **2016**, *237*, 59−66.
(12) Almassio, M. F.; Romagnoli, M. J.; Del Rosso, P. G.; Schvval, A. B.; Garay, R. O. Distyrylbenzene-based Segmented Conjugated Polymers: Synthesis, Thin Film Morphology and Chemosensing of Hydrophobic and Hydrophilic Nitroaromatics in Aqueous Media. *Polymer* **2017**, *113*, 167−179.
(13) Hu, J.; Liu, R.; Zhai, S.; Wu, Y.; Zhang, H.; Cheng, H.; Zhu, H. AIE-active Molecule-based Self-assembled Nano-fibrous Films for Sensitive Detection of Volatile Organic Amines. *J. Mater. Chem. C* **2017**, *5*, 11781−11789.
(14) Lamnatou, C.; Chemisana, D. Solar Radiation Manipulations and Their Role in Greenhouse Claddings: Fluorescent Solar Concentrators, Photoselective and Other Materials. *Renewable Sustainable Energy Rev.* **2013**, *27*, 175−190.
(15) Lin, Z.; Zhang, J.; Ma, H.; Yao, Z. Preparation and Properties of Polymerizable 1,8-naphthalimide Fluorescent Dye Grafted Linear Low-density Polyethylene. *J. Appl. Polym. Sci.* **2015**, *132*, 42172.
(16) Petrović, S.; Zvezdanović, J.; Marković, D. Chlorophyll Degradation in Aqueous Mediums Induced by Light and UV-B Irradiation: An UHPLC-ESI-MS Study. *Radiat. Phys. Chem.* **2017**, *141*, 8−16.
(17) Kondratyev, K. Y. *Radiation in the Atmosphere*. Academic Press: New York, 1969.
(18) White, A. L.; Jahnke, L. S. Contrasting Effects of UV-A and UV-B on Photosynthesis and Photoprotection of β-carotene in Two Dunaliella Spp. *Plant Cell Physiol.* **2002**, *43*, 877−884.
(19) Jung, H.-S.; Kim, Y.-J.; Ha, S.-W.; Lee, J.-K. White Light-emitting Diodes Using Thermally and Photochemically Stable Fluorescent Silica Nanoparticles as Color-converters. *J. Mater. Chem. C* **2013**, *1*, 5879−5884.
(20) Wang, B.; Zhang, A.; Jia, J.; Xu, W.; Shen, Q.; Liu, X.; Jia, H. A Novel Red Emitting Polymeric Complex as a Directly Film-forming Phosphor Applied in NUV-based LEDs. *Opt. Mater.* **2017**, *73*, 772−780.
(21) Di Martino, D.; Beverina, L.; Sassi, M.; Brovelli, S.; Tubino, R.; Meinardi, F. Straightforward Fabrication of Stable White LEDs by Embedding of Inorganic UV-LEDs into Bulk Polymerized Polymethyl-methacrylate Doped with Organic Dyes. *Sci. Rep.* **2014**, *4*, 4400.
(22) Kim, J.-H.; Kim, K.-S.; Yoo, S. I.; Sohn, B.-H. Dispersion of micelle-encapsulated fluorophores in a polymer matrix for control of color of light emitted by light-emitting diodes. *Thin Solid Films* **2011**, *519*, 8161−8165.
(23) Zhang, Q.; Wang, C.-F.; Ling, L.-T.; Chen, S. Fluorescent nanomaterial-derived white light-emitting diodes: what's going on. *J. Mater. Chem. C* **2014**, *2*, 4358−4373.
(24) Chang, K.; Men, X.; Chen, H.; Liu, Z.; Yin, S.; Qin, W.; Yuan, Z.; Wu, C. Silica-encapsulated semiconductor polymer dots as stable phosphors for white light-emitting diodes. *J. Mater. Chem. C* **2015**, *3*, 7281−7285.
(25) Fasol, G.; Nakamura, S. *The Blue Laser Diode: GaN Based Blue Light Emitters and Lasers*; Springer: Berlin, 1997.
(26) Senden, T.; van Dijk-Moes, R. J. A.; Meijerink, A. Quenching of The Red Mn^{4+} Luminescence in Mn^{4+}-doped Fluoride LED Phosphors. *Light Sci. Appl.* **2018**, *7*, 8.
(27) Song, E.; Wang, J.; Shi, J.; Deng, T.; Ye, S.; Peng, M.; Wang, J.; Wondraczek, L.; Zhang, Q. Highly Efficient and Thermally Stable K_3AlF_6:Mn^{4+} as a Red Phosphor for Ultra-High-Performance Warm White Light-Emitting Diodes. *ACS Appl. Mater. Interfaces* **2017**, *9*, 8805−8812.
(28) Huang, L.; Zhu, Y.; Zhang, X.; Zou, R.; Pan, F.; Wang, J.; Wu, M. HF-Free Hydrothermal Route for Synthesis of Highly Efficient Narrow-Band Red Emitting Phosphor $K_2Si_{1-x}F_6$:xMn^{4+} for Warm White Light-Emitting Diodes. *Chem. Mater.* **2016**, *28*, 1495−1502.
(29) Muramoto, Y.; Kimura, M.; Nouda, S. Development and Future of Ultraviolet light-emitting Diodes: UV-LED Will Replace The UV Lamp. *Semicond. Sci. Technol.* **2014**, *29*, 084004.
(30) Steigerwald, D. A.; Bhat, J. C.; Collins, D.; Fletcher, R. M.; Holcomb, M. O.; Ludowise, M. J.; Martin, P. S.; Rudaz, S. L. Illumination with Solid State Lighting Technology. *IEEE J. Sel. Top. Quant.* **2002**, *8*, 310−320.
(31) Sheu, J. K.; Chang, S. J.; Kuo, C. H.; Su, Y. K.; Wu, L. W.; Lin, Y. C.; Lai, W. C.; Tsai, J. M.; Chi, G. C.; Wu, R. K. White-light Emission from Near UV InGaN-GaN LED Chip Precoated with Blue/green/red Phosphors. *IEEE Photonics Technol. Lett.* **2003**, *15*, 18−20.
(32) Cho, J.; Park, J. H.; Kim, J. K.; Schubert, E. F. White Light-emitting Diodes: History, Progress, and Future. *Laser Photon. Rev.* **2017**, *11*, 1600147.
(33) Ye, S.; Xiao, F.; Pan, Y. X.; Ma, Y. Y.; Zhang, Q. Y. Phosphors in Phosphor-converted White Light-emitting Diodes: Recent Advances in Materials, Techniques and Properties. *Mater. Sci. Eng., R* **2010**, *71*, 1−34.
(34) Li, G.; Tian, Y.; Zhao, Y.; Lin, J. Recent Progress in Luminescence Tuning of Ce^{3+} and Eu^{2+}-activated Phosphors for pc-WLEDs. *Chem. Soc. Rev.* **2015**, *44*, 8688−8713.
(35) Lin, C. C.; Liu, R.-S. Advances in Phosphors for Light-emitting Diodes. *J. Phys. Chem. Lett.* **2011**, *2*, 1268−1277.
(36) Lin, Y.-C.; Karlsson, M.; Bettinelli, M. Inorganic Phosphor Materials for Lighting. *Top. Curr. Chem.* **2016**, *374*, 21.
(37) Xia, Z.; Xu, Z.; Chen, M.; Liu, Q. Recent Developments in the New Inorganic Solid-state LED Phosphors. *Dalton Trans.* **2016**, *45*, 11214−11232.
(38) Li, J.; Yan, J.; Wen, D.; Khan, W. U.; Shi, J.; Wu, M.; Su, Q.; Tanner, P. A. Advanced Red Phosphors for White Light- emitting Diodes. *J. Mater. Chem. C* **2016**, *4*, 8611−8623.
(39) Lee, J. C.; Jeong, Y.-K.; Kim, J.-M.; Kang, J.-G. Sensitized Luminescence of Eu(III) Complexes with Schiff-base and 1, 10-phenanthroline: Role of Schiff-base As a Sensitizer. *Spectrochim. Acta, Part A* **2014**, *124*, 256−264.
(40) Kang, J.-S.; Jeong, Y.-K.; Shim, Y. S.; Rout, S.; Leung, K. T.; Sohn, Y.; Kang, J.-G. Structures, and Luminescence and Magnetic properties of Ln(III) Complexes Bearing Dibenzoylmethane Ligand (Ln=Eu and Gd). *J. Lumin.* **2016**, *178*, 368−374.
(41) Kang, J.-S.; Leung, K. T.; Cho, H.-K.; Kang, J.-G.; Sohn, Y. Luminescence and Magnetic Properties of Tb(III) Complexes with TETA and Synergistic Effect by 1, 10-Phenanthroline. *Bull. Korean Chem. Soc.* **2016**, *37*, 1458−1463.
(42) Gao, X.; Chang, S.; Liu, H.; Liu, Z. A Promising White-Light-Emitting Material Constructed from Encapsulating Eu^{3+}/Tb^{3+} Hybrid Ions into a Robust Microporous Metal-Organic Framework. *Eur. J. Inorg. Chem.* **2016**, 2837−2842.

DOI: 10.1021/acsami.8b17256
ACS Appl. Mater. Interfaces 2018, 10, 44768−44775

(43) Kumar, P.; Soumya, S.; Prasad, E. Enhanced Resonance Energy Transfer and White-Light Emission from Organic Fluorophores and Lanthanides in Dendron-based Hybrid Hydrogel. *ACS Appl. Mater. Interfaces* **2016**, *8*, 8068−8075.
(44) Lee, H.-Y.; Kim, K.-W.; Park, C.-E.; Kim, G.-H.; Choi, J.-H. Novel Ethyne-linked Compounds Containing 1,8-naphthalimide Group for Light Conversion Film. *MATEC Web Conf.* **2016**, *67*, 01016.
(45) Yang, C.; Zhou, H.; Xu, J.; Li, Y.; Lu, M.; He, J.; Zhang, Q. A Series of Highly Quantum Efficiency PMMA Luminescent Films Doped with Eu-complex as Promising Light-conversion Molecular Devices. *J. Mater. Sci.: Mater. Electron.* **2016**, *27*, 11284−11292.
(46) Liu, L.; Yu, M.; Zhang, J.; Wang, B.; Liu, W.; Tang, Y. Facile Fabrication of Color-tunable and White Light Emitting Nanocomposite Films Based on Layered Rare-earth Hydroxides. *J. Mater. Chem. C* **2015**, *3*, 2326−2333.
(47) Huang, M.-R.; Li, X.-G. Thermal Degradation of Cellulose and Cellulose Esters. *J. Appl. Polym. Sci.* **1998**, *68*, 293−304.
(48) Puls, J.; Wilson, S. A.; Hölter, D. Degradation of Cellulose Acetate-Based Materials: A Review. *J. Polym. Environ.* **2010**, *19*, 152−165.
(49) Cozzi, P. G. Metal-Salen Schiff Base Complexes in Catalysis: Practical Aspects. *Chem. Soc. Rev.* **2004**, *33*, 410−421.
(50) Frisch, M. J.; Trucks, G. W.; Schlegel, H. B.; Scuseria, G. E.; Robb, M. A.; Cheeseman, J. R.; Scalmani, G.; Barone, V.; Mennucci, B.; Petersson, G. A.; Nakatsuji, H.; Caricato, M.; Li, X.; Hratchian, H. P.; Izmaylov, A. F.; Bloino, J.; Zheng, G.; Sonnenberg, J. L.; Hada, M.; Ehara, M.; Toyota, K.; Fukuda, R.; Hasegawa, J.; Ishida, M.; Nakajima, T.; Honda, Y.; Kitao, O.; Nakai, H.; Vreven, T.; Montgomery, J. A., Jr.; Peralta, J. E.; Ogliaro, F.; Bearpark, M.; Heyd, J. J.; Brothers, E.; Kudin, A.; Staroverov, V. N.; Kobayashi, R.; Normand, J.; Raghavachari, K.; Rendell, A.; Burant, J. C.; Iyengar, S. S.; Tomasi, J.; Cossi, M.; Rega, N.; Millam, J. M.; Klene, M.; Knox, J. E.; Cross, J. B.; Bakken, V.; Adamo, C.; Jaramillo, J.; Gomperts, R.; Stratmann, R. E.; Yazyev, O.; Austin, A. J.; Cammi, R.; Pomelli, C.; Ochterski, J. W.; Martin, R. L.; Morokuma, K.; Zakrzewski, V. G.; Voth, G. A.; Salvador, P.; Dannenberg, J. J.; Dapprich, S.; Daniels, A. D.; Farkas, O.; Foresman, J. B.; Ortiz, J. V.; Cioslowski, J.; Fox, D. J. *Gaussian 09*, Revision A.02; Gaussian, Inc.: Wallingford CT, 2009.
(51) Kim, K.-B.; Kim, Y.-I.; Chun, H.-G.; Cho, T.-Y.; Jung, J.-S.; Kang, J.-G. Structural and Optical Properties of $BaMgAl_{10}O_{17}:Eu^{2+}$ Phosphor. *Chem. Mater.* **2002**, *14*, 5045−5052.
(52) Blasse, G. Thermal Quenching of Characteristic Luminescence. II. *J. Solid State Chem.* **1974**, *9*, 147−151.
(53) Stein, G.; Würzberg, E. Energy Gap Law in the Solvent Isotope Effect on Radiationless Transitions of Rare Earth Ions. *J. Chem. Phys.* **1975**, *62*, 208.

DOI: 10.1021/acsami.8b17256
ACS Appl. Mater. Interfaces 2018, 10, 44768−44775